Quantitative Characterization of Ion Pairing and Cluster Formation in Strong 1:1 Electrolytes

Alan A. Chen[†] and Rohit V. Pappu*[,†,‡]

Molecular Biophysics Program & Center for Computational Biology, Washington University School of Medicine, St. Louis, Missouri 63110, and Department of Biomedical Engineering & Center for Computational Biology, Washington University in St. Louis, One Brookings Drive, Campus Box 1097, St. Louis, Missouri 63130

Received: January 31, 2007; In Final Form: March 10, 2007

Aqueous solutions of 1:1 strong electrolytes are considered to be the prototype for complete ionic dissociation. Nonetheless, clustering of strong 1:1 electrolytes has been widely reported in all atom molecular dynamics simulations, and their presence is indirectly implicated in a diverse range of experimental results. Is there a physical basis for nonidealities such as ion pairing and cluster formation in aqueous solutions of strong 1:1 electrolytes? We attempt to answer this question by direct comparison of results from detailed molecular dynamics simulations to experimentally observed properties of 1:1 electrolytes. We report the analysis of a series of lengthy molecular dynamics simulations of alkali−halide solutions carried out over a wide range of physiologically relevant concentrations using explicit representations of water molecules. We find evidence for pronounced nonideal behavior of ions at all concentrations in the form of ion pairs and clusters which are in rapid equilibrium with dissociated ions. The phenomenology for ion pairing seen in these simulations is congruent with the multistep scheme proposed by Eigen and Tamm based on data from ultrasonic absorption experiments. For a given electrolyte, we show that the dependence of cluster populations on concentration can be described through a single set of equilibrium constants. We assess the accuracy of calculated ion pairing constants by favorable comparison to estimates obtained by Fuoss and co-workers and based on conductometric experiments. Ion pairs and clusters form on length scales where the size of individual water molecules is as important as the hard core radius of ions. Ion pairing results as a balance between the favorable Coulomb interactions and the unfavorable partial desolvation of ions needed to form a pair.

Introduction

Ion pairing and clustering are recurring albeit controversial themes in the physical chemistry of electrolytes.[1−7] Evidence of ion pairing is well-documented for asymmetric, multivalent, and multi-atomic salts,[1−5,7] whereas aqueous solutions of 1:1 strong electrolytes are designated as prototypes for complete ionic dissociation.[1,8] Conversely, data from conductometry,[9,10] potentiometry,[11] NMR,[12] and dynamic light scattering[13] experiments as well as reports from molecular dynamics simulations[14−20] provide evidence for pairing and cluster formation in an aqueous solution of strong 1:1 electrolytes. Is there a physical basis for these reports of nonidealities? We attempt to answer this question by direct comparison of data from detailed molecular dynamics simulations of electrolyte solutions to estimates based on data from conductometric[9] and ultrasonic absorption experiments.[21] If clustering is in fact real, it may explain the origin of the excess ionic activity in 1:1 electrolytes, which in turn is thermodynamically linked to the conformational and binding equilibria of nucleic acids.[22−25]

Classical models for aqueous solutions of strong 1:1 electrolytes are based on one of two approaches for modeling ionic interactions, namely, the Debye−Hückel model[26] (D−H) and the Primitive model[1] (PM). In these models, water is treated as a featureless, homogeneous medium characterized by a dielectric constant of approximately 80 at 25 °C. Bjerrum showed that ion pairing in these models for 1:1 strong electrolytes depends on the value one assumes for the dielectric constant.[1,2,27] Specifically, if the dielectric constant is greater than 40, then the electrolyte is characterized by negligible ion pairing. This is because the Coulomb attraction is diminished by the bulk dielectric, a feature which is presumed to hold irrespective of the length scale separating a pair of oppositely charged ions.

Predictions based on D−H and PM fail to explain the concentration dependence of a range of colligative properties of 1:1 electrolytes past the infinite dilution limit.[1,8,28] Yet, the assumption of complete ionic dissociation is often applied over a wide range of concentrations.[1,8] Ion pairs and clusters form on length scales where the size of individual water molecules is as important as the hard core radius of ions (∼3−7 Å). Although a reasonable model for electrolytes should reproduce predictions of the D−H model at infinite dilution, there is no a priori reason to expect that the D−H assumptions are valid at higher concentrations.

The state-of-the-art analytical models for strong electrolytes are based on integral equation methods, in which deviations from a reference system are described as a series of multi-body correlation functions. With the proper choice of reference systems, the short range behavior of a Lennard−Jones fluid can be combined with the long-range correlations from classical continuum models,[8] thus addressing the lack of solvent granu-

* To whom correspondence should be addressed. E-mail: pappu@biomed.wustl.edu.
[†] Molecular Biophysics Program & Center for Computational Biology.
[‡] Department of Biomedical Engineering & Center for Computational Biology.

10.1021/jp0708547 CCC: $37.00
Published on Web 05/23/2007

larity in the latter. This advance allows integral equation models to faithfully reproduce thermodynamic properties of aqueous strong electrolytes to significantly higher concentrations than the limiting laws.[8,29,30] For a comprehensive discussion of ion pairing in integral equation methods, readers are directed to the recent review by Marcus and Hefter[1] and the treatise of Barthel et al.[8]

However, integral equation methods fail at high (~1 M) concentrations,[8] presumably because water is a polar, anisotropic molecule with significantly different behavior than a simple Lennard−Jones fluid. Advanced integral equation methods capable of treating the site-specific correlations of polyatomic molecules are necessary to capture the hydrogen-bonding nature of water.[31] Capturing the solvation thermodynamics of ions in such frameworks requires many additional considerations beyond the scope of this discussion, and readers are directed to recent work of Kovalenka and Hirata[29] (and references therein) for a summary of progress in the field. In principle, any amount of deviation from ideality may be captured given sufficient many-body correlations. However, there is no consensus on what the correct short-range correlations should be for an aqueous strong electrolyte.[1] These many-body correlations cannot be obtained from experiments. Instead, the refinement of theory proceeds through comparison to data extracted from all-atom computer simulations. In this approach, one implicitly assumes that data from all-atom simulations themselves are sufficiently accurate.

As noted above, ion pairing and clustering have been observed in atomistic simulations of electrolytes and of polyelectrolytes in excess monovalent salts. Do these observations meet the standard of being quantitatively accurate; that is, are the nonidealities observed in molecular simulations consistent with estimates based on measurements of thermodynamic and transport properties of 1:1 electrolytes? We answer this question through analysis of data from a series of lengthy molecular dynamics simulations of alkali−halide solutions. These simulations were carried out over a wide range of biologically relevant concentrations using explicit representations of water molecules. We find evidence for pronounced nonideal behavior of ions at all concentrations. Prior to describing the methodology employed in this work and the results derived from our analysis, we provide a summary of results from conductometric measurements on 1:1 electrolytes, which provides the framework for a quantitative comparison between our results and those from experiment.

Conductometry and Ion Pairing. Consequences of nonidealities caused by ion pairing can be directly measured as a deficit in the rate of charge transport. The conductance per equivalent of electrolyte (specific conductance) decreases with increasing concentration from a limiting value at infinite dilution. The specific conductance Λ of an ionic solution is defined as the ratio of the current density to the magnitude of the applied electric field. Debye and Hückel postulated that strong electrolytes are fully dissociated and are able to interact with one another through an ion cloud embedded in a bulk dielectric.[26] Onsager calculated the electrophoretic viscosity of an ion in its "ionic atmosphere" as a function of concentration, and this led to the Debye−Hückel−Onsager (DHO) conductance equation:[32]

$$\Lambda = \Lambda_0 - S_1(c)^{(1/2)} - S_2\Lambda_0 \quad (1)$$

Here, c is the salt concentration, Λ_0 is the limiting conductance at infinite dilution, and S_1 and S_2 are fixed parameters derived from the dielectric friction theory.[32] The DHO equation assumes that any diminution in conductance with increasing concentration is due entirely to a decrease in the average ion velocity resulting from an increase in ionic viscosity. The ratio of charge carriers to concentration is assumed to be constant and equal to one. Experimentally, this law was found to be exact for strong electrolytes at infinite dilution but was inaccurate at concentrations greater than 0.005 equiv per liter.[5]

Fuoss and Onsager extended the concentration range of the DHO equations by retaining higher order terms in the relaxation and electrophoresis expressions.[33] While this improvement resulted in agreement with experiment up to concentrations of 0.01 equiv per liter, the modest gain in accuracy came at the cost of substantially increased mathematical complexity. Realizing that a featureless continuum could never correctly capture short-range ion−solvent interactions, Fuoss questioned the Debye−Hückel assumption of complete ionic dissociation. He reasoned that ion pairing could contribute to a depletion of charge carriers in the ensemble average. This led to development of the Fuoss−Hsia conductance equations,[34] which contain both a DHO-like viscosity change and a mass-action pairing term as shown in eq 2:

$$\Lambda = \alpha\{\Lambda_0 - S(\alpha c)^{1/2} + E\alpha c \ln(\alpha c) + J_1\alpha c - J_2(\alpha c)^{3/2}\} \quad (2)$$

Here, α is the dissociation coefficient, and c is the total concentration of the electrolyte. S, E, J_1, and J_2 are derived from theoretical expressions for the electrophoretic mobility and dielectric relaxation and depend only on the dielectric constant, the viscosity of the solvent, and the hydrodynamic radii of the ions. Λ_0 is the limiting conductance at infinite dilution, which can be determined independently using low concentration data and the DHO limiting law. The degree of dissociation, α, is a fitted parameter which accounts for the fraction of nonconducting ion pairs; this parameter is converted to an association constant K_a by fitting data over a concentration range. The only other fitted parameter is the hydrodynamic radius of an ion, which enters in the expressions for J_1 and J_2 and should be constant for a given solvent. The concentration-dependent viscosity only applies to the *free* electrolyte fraction while the pairs are assumed to be conductively inert.

The F−H conductance equations[34] (and subsequent revisions)[35−38] are appealing because they employ the fewest number of ad hoc parameters. Using these equations, Fuoss was able to reproduce electrolyte conductivities up to ~0.1 equiv per liter of solvent regardless of electrolyte "strength" or solvent type.[9] This upper limit coincides with Fuoss' estimate for the minimum concentration necessary for the formation of ion triplets in aqueous solution under ambient conditions.[39,40] The validity of the F−H equations has an upper limit because large clusters such as triplets and quintuplets have a net charge and therefore contribute an unknown amount to the conductivity. Additionally, larger, neutral clusters such as quadruples and sextuples are likely to influence both the viscosity of the solution and the response of the solution to external fields. These effects influence the interpretation of conductivity measurements in unknown ways.

Methods

We report results from analysis of multiple, long molecular dynamics simulations for eight different 1:1 electrolytes. We carried out simulations for aqueous solutions of NaCl and KCl at concentrations equivalent to 100 m*m*, 250 m*m*, 500 m*m*, 750 m*m*, and 1 *m* where *m* denotes molality. In addition, we carried

TABLE 1: Parameters Used to Model Lennard−Jones Interactions of Anions and Cations in Conjunction with the Mixing Rules That Are Part of the OPLS/AA Forcefield

ion	σ (Å)	ϵ (kJ mol^{-1})	literature reference
Na^+	3.33045	1.15980×10^{-2}	Aqvist[42]
K^+	4.93463	1.37235×10^{-3}	Aqvist[42]
Rb^+	5.62177	7.15464×10^{-4}	Aqvist[42]
Cs^+	6.71600	3.38904×10^{-4}	Aqvist[42]
Cl^-	4.41724	4.92833×10^{-1}	Chandresekhar et al.[60]
Br^-	4.62376	3.76560×10^{-1}	Lybrand et al.[61]

out simulations for 1 *m* aqueous solutions of the electrolytes NaBr, KBr, RbCl, RbBr, CsCl, and CsBr.

Details of the Forcefield. Ions were modeled using parameters that are part of the all atom OPSL/AA forcefield.[41] The Group I cation parameters in this forcefield are adaptations of values originally obtained by Aqvist.[42] In Table 1, we provide details of the ion forcefield parameters used in our simulations. For water molecules, we used the rigid 3-site TIP3P model.[43] The ion parameters developed by Aqvist are available for a wide variety of alkali metals.[42] The paradigm used by Aqvist to obtain parameters for the Lennard−Jones 12-6 potential is identical for all Group I cations. This allowed us to carry out a systematic analysis of how nonidealities such as ion pairing and cluster formation vary with cation size.

Details of the Molecular Dynamics Simulations. All molecular dynamics simulations were performed using version 3.3 of the GROMACS molecular dynamics package.[44] All simulations used the isothermal−isobaric ensemble, that is, constant pressure of 1 bar and temperature of 298 K. The weak coupling algorithms of Berendsen and co-workers were used for both the manostat and the thermostat,[45] with coupling constants of 1 ps and 0.2 ps, respectively. The equations of motion were integrated using a 2 fs time step and the leapfrog algorithm.[46] The two bond lengths and one bond angle in each water molecule were constrained to values prescribed by the TIP3P model using the SETTLE algorithm of Miyamoto and Kollman.[47] Snapshots were saved for analysis once every 2 ps. For each of our electrolyte simulations, we generated four independent 10 ns trajectories. Each of the four trajectories was generated using different, randomized starting coordinates and velocities. We settled on the choice of four trajectories of length 10 ns each based on the sizes of error bars obtained from the bootstrap analysis, the details of which are described in the latter part of this section. The 10 ns per trajectory is in excess of the initial 2 ns used for equilibration of the simulation cells prepared as described below. The length of each simulation merits some discussion. In simulations of 22 neutralizing counterions around double-stranded DNA, Ponomarev et al.[48] have shown that macroion−counterion pair correlation functions converge on the time scale of approximately 10 ns. Our simulations differ in two ways: First, the absence of a macroion decreases the time required to obtain converged ion−ion pair correlation functions. For instance, the Na−Cl, Na^+-Na^+, and Cl^--Cl^- pair correlation functions in simulations of 1 *m* solutions converge to their equilibrium distributions within a time scale of approximately 1 ns. This conclusion was reached using an analysis identical to that of Ponomarev et al.[48] Second, our most reliable estimates for pairing and clustering equilibrium constants are obtained using the 1 *m* simulations. In these simulations, there are 204 ions of each type, and the statistics we obtain are reliable when compared to simulations based on the use of fewer ions.

We used periodic boundary conditions to mimic the macroscopic setting for electrolytes. This choice represents a departure from that of Aqvist[42] who used spherical droplets in conjunction with the surface constraint all-atom model of Warshel and King.[49] In order to accurately capture the behavior of bulk electrolyte solutions, we required simulation cells that were sufficiently large to minimize finite-size artifacts.[50] In all of our simulations, the central simulation cell was a cubic box approximately 71 Å on a side. Long-range electrostatic interactions between periodic images were treated using the particle mesh Ewald approach.[51] We used fourth-order cubic interpolation with a tolerance of 10^{-5}. Neighbor lists were updated every 10 time steps. A cutoff of 10 Å was used for van der Waals interactions, real space Coulomb interactions, and for updating neighbor lists.

Generating Starting Coordinates for Electrolyte Solutions. In all of our simulations, the number of water molecules was set to be $N_W = 11\,341$. This number was chosen because it corresponds to a density of 1 g/cm^3 when water molecules are enclosed in a cubic box of side 70 Å. To simulate an electrolyte solution of a particular concentration, equal numbers of anions and cations were added to the periodic box according to the molal scale. We use the molal scale to maintain consistency with the scales used in conductometric experiments and in measurements of activity coefficients. Additionally, the molal scale is preferred to the molar scale because our simulations are carried out in the isothermal, isobaric ensemble, with a fixed number of particles and fluctuating volumes. The relationship between molality and the number of cations/anions is $m = 4.894 \times 10^{-3} N_{ion}$ for $N_W = 11\,341$. Here, *m* is the desired molality, N_{ion} is the number of anions/cations that are to be added to the simulation box, and the numerical prefactor derives from the requirement that water should be 55.5 molal with respect to itself. To prepare the periodic box, we first generated an equilibrated box of the neat liquid with the requisite excess number of water molecules, that is, $11\,341 + 2N_{ion}$. The snapshot obtained at the end of an equilibration run was modified by randomly replacing the excess $2N_{ion}$ water molecules with N_{ion} anions and N_{ion} cations, respectively. In our setup, a bulk concentration of 1 *m* was simulated using 11 341 water molecules and 204 cations and anions, respectively ($N_{ion} = 204$). To simulate electrolytes at other concentrations, the number of water molecules was held fixed, and the numbers of cations/anions were adjusted using the conversion factor described above. To rule out the possibility that our results are a consequence of finite size artifacts, we also carried out a single set of reference simulations using 27 750 water molecules with 50 anions and cations to mimic a solution of 0.1 *m* NaCl. Data from these simulations are quantitatively similar to data gathered using smaller periodic boxes (data not shown). For each simulation, an initial equilibration in the NPT ensemble was carried out for a period of 2 ns.

Quantitative Criteria for Identifying Ion Pairs and Clusters. Two ions were considered to form an ion pair if their interatomic distance was less than a prescribed cutoff. The cutoffs were set at the distance corresponding to the minimum between the first and second peaks of the solution average cation−anion radial distribution function (RDF). The values of the cutoffs used for each cation−anion combination are given in Table 2. Clusters were defined as groups of ions topologically connected by pairing interactions; that is, all members of the same cluster are reachable via successive pairing contacts. In our analysis, we did not place any restriction on the geometry or maximum size of an allowable cluster.

Quantification of Equilibria between Fully Solvated Ions and Partially Desolvated Clusters. We have applied the law of mass action to quantify ion pairing and cluster equilibria in

TABLE 2: Locations of First and Second Minima and Maxima in RDFs for Each of the Eight Strong 1:1 Electrolytes[a]

salt	$r^{(1)}_{max}$ (Å)	$r^{(1)}_{min}$ (Å)	$r^{(2)}_{max}$ (Å)	$r^{(2)}_{min}$ (Å)
NaCl	2.74	3.60	5.20	6.15
NaBr	2.75	3.75	5.30	6.20
KCl	3.10	4.10	5.45	6.50
KBr	3.15	4.15	5.55	6.60
RbCl	3.23	4.25	5.55	6.60
RbBr	3.28	4.30	5.60	6.75
CsCl	3.48	4.50	5.70	6.90
CsBr	3.51	4.55	5.80	7.00

[a] The data were extracted from RDFs computed for electrolyte concentrations of 1 *m*.

different 1:1 electrolytes. The necessary equilibrium constants were computed using statistics for the numbers of pairs and higher order clusters that we obtain from a set of uncorrelated snapshots. These cluster statistics were then converted to molal concentrations in order to calculate the relative equilibrium constants. As an example, pair association constants $k_{1,1}$ were computed as $k_{1,1} = [CA]/[C][A]$ where [CA] denotes the molal concentration of ion pairs while [C] and [A] are molal concentrations of cations and anions, respectively.

Bootstrap Analysis. Adjacent snapshots along a molecular dynamics simulation trajectory tend to be highly correlated with each other. To assess the characteristic time scale for the loss of such correlations, we needed to measure the relaxation times associated with the phenomena of interest. The time scale of interest was the characteristic time for an ion pair to become uncorrelated. Ion pairs frequently dissociate only to migrate in a correlated fashion and then reassociate shortly thereafter, and these should not be treated as two independent pairing events. Therefore, a simplistic tabulation of ion pair lifetimes does not suffice to estimate the true pair decorrelation time τ. In order to accurately quantify the loss of pairing memory, we first identify all unique ion pairs that form over the course of a simulation. We define an ion pair relaxation function as

$$G_m(r, t) = \frac{V}{N_{pairs}^2} \left\langle \sum_{pairs} \delta(r - ||\boldsymbol{R}_i(t) - \boldsymbol{R}_j(t)||) \right\rangle \qquad (3)$$

Here, $G_m(r, t)$ is the relative probability per unit volume of finding a tagged ion pair to be separated by distance r at time t, given that this pair initially formed at $t = 0$; $\boldsymbol{R}_i(t)$ and $\boldsymbol{R}_j(t)$ are position vectors at time t for ions i and j, respectively, as shown in Figure 1. Our definition of $G_m(r, t)$ is analogous to the time-dependent correlation function proposed by van Hove.[52] The characteristic time τ is determined by measuring the rate of decay of the area under the first peak to its asymptotic value, which is simply the average cation−anion RDF. If the decay of $G_m(r, t)$ can be fit to a single exponential, then τ is the time scale elapsed before the van Hove correlation function converges to 1/e of the asymptotic value for the equilibrium pair correlation function. Alternatively, the decay of $G_m(r, t)$ may be a multiexponential process. In this scenario, the time scale of interest is that of the slowest process denoted as τ_s. The task of identifying uncorrelated samples reduces to picking snapshots that are at least $2\tau_s$ apart along a trajectory. As noted above, for each electrolyte simulation, we generated four independent trajectories. Information regarding ion pair decorrelation times was used in conjunction with bootstrap analysis to estimate pair and cluster equilibrium constants according to the following protocol: 1. A trajectory was chosen at random; 2. A set of snapshots corresponding to a time scale of $2\tau_s$ was discarded as equilibration; 3. A random starting snapshot was then picked and statistics for the quantities were gathered; 4. Subsequent snapshots chosen for the analysis were spaced $2\tau_s$ apart, until the end of the trajectory, and combined to form a single subsample; 5. We return to step 1 and repeat steps 1−4 for approximately 200 bootstrap subsamples.

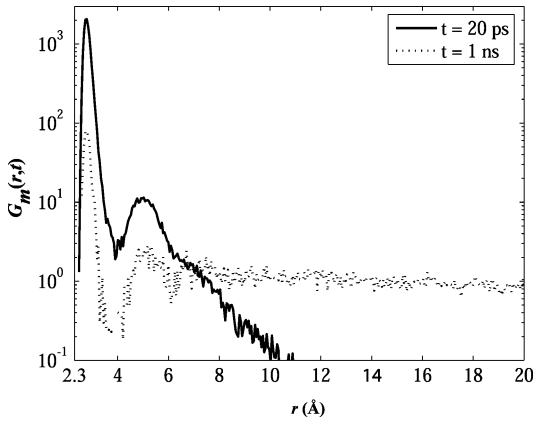

Figure 1. Illustration of the time-dependent ion pair decorrelation. The solid curve shows $G_m(r, t = 20$ ps) and the dashed curve shows the $G_m(r, t = 1$ ns). The latter converges to the equilibrium cation−anion RDF.

Averages and standard deviations for estimates of means were calculated using the subsamples generated from bootstrap sampling.

Results and Discussions

Nonidealities Apparent in Analysis of Radial Distribution Functions. Figure 2 shows cation−anion, cation−cation, and anion−anion RDFs for NaCl across a range of concentrations. Similar results were obtained for KCl (data not shown). The RDFs depend on electrolyte concentration in counterintuitive ways: specifically, the degree of cation−anion correlations is found to decrease with increasing concentration, while both the cation−cation and anion−anion RDFs exhibit the onset of short-range correlations. We reasoned that the origin of increasing correlations between like-charged ions must result from the increased likelihood of populating ion triplets and higher order clusters at higher concentrations. In fact, the triplets consist of two like-charged ions bridged by an intervening ion of the opposite charge, which leads to an apparent correlation between like-charged ions. In light of the nonidealities apparent at the level of RDFs, we analyzed the simulation data to quantify the likelihood of forming pairs and higher order clusters.

Cluster Based Model for Describing the Nonidealities of 1:1 Strong Electrolytes. We used the law of mass action to describe cluster equilibria because cluster populations maintained strict time-average ratios. The equilibrium constants between the free ions and the various clusters were calculated using the ensemble average cluster populations, resulting in a network of association equilibria as shown in Figure 3. We assume that all reactions are bimolecular; that is, higher order clusters are formed by stepwise addition to smaller clusters. Since free ions and ion pairs are the dominant species at all concentrations, we consider only additions of free ions or ion pairs. This yielded a network of equilibrium constants diagrammed in Figure 3. The computed equilibrium constants should satisfy two requirements: they should be independent of concentration, and they should allow us to accurately predict the cluster populations at arbitrary concentrations.

As reported in Table 3, the cluster association constants are indeed independent of concentration for NaCl and KCl. While

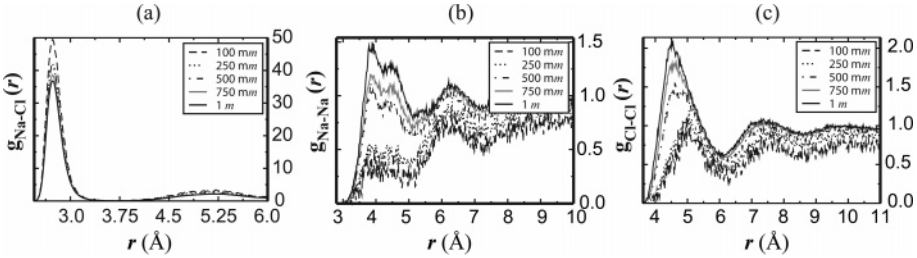

Figure 2. Concentration-dependent RDFs for NaCl. The RDFs are as follows: (a) Na−Cl; (b) Na−Na; and (c) Cl−Cl. The concentrations are shown in the inset for each panel.

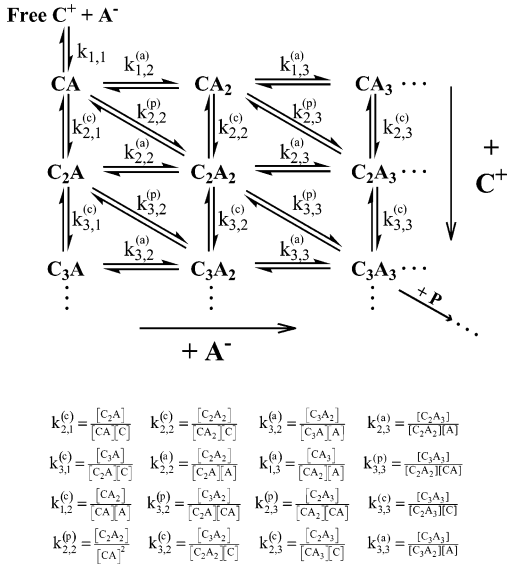

Figure 3. Schematic of reaction scheme used to analyze nonidealities in the simulated 1:1 electrolytes. Only clusters of size ≤6 need be considered for concentrations up to 1 *m*, but higher concentrations require consideration of larger clusters. Only bimolecular reactions are considered, so a new cluster is formed either through unilateral associations, that is, addition of an anion or a cation, or bilateral associations, that is, addition of an ion pair. Definitions of the microscopic equilibrium constants are shown in the lower panel. The notational convention for equilibrium constants is as follows: C ≡ cation, A ≡ anion, and the subscripts refer to the number of each in the cluster that is formed. Clusters with unequal numbers of anions and cations have a net charge. The superscripts are used to denote clusters formed by the addition of anions (a), cations (c), or pairs (p). Square brackets denote concentration on the molal scale.

this may seem trivial, it should be noted that Arrhenius' original model for strong electrolytes[53] invoked ion pairing that did not obey the law of mass action. Similarly, previous attempts to quantify pairing in electrolyte simulations did not distinguish between ion pairs and higher order clustering. This also resulted in association "constants" which varied with concentration.[15−17,54] The fact that our equilibrium constants obey mass action indicates that our approach of separating by cluster type represents a thermodynamically consistent way of partitioning the whole salt into distinct microstates.

The second criterion to justify the mass action approach is the degree to which tabulated equilibrium constants can be used to accurately predict cluster populations at concentrations other than the one from which the equilibrium constants were extracted. To test this, we have numerically calculated the predicted cluster populations at 100, 250, 500, and 750 m*m* using the equilibrium constants extracted from 1 *m* simulations of NaCl and KCl. These were compared to the actual measured cluster populations from simulation. Results of this comparative analysis are shown in Figure 4. The predicted populations are identical to the measured populations. At low concentrations, clusters larger than pairs are not populated for NaCl and KCl. At higher concentration, there is an increase in the likelihood of observing larger clusters, and there are discernible differences between NaCl and KCl. In principle, an exhaustively sampled dilute electrolyte simulation would eventually yield all of the higher order equilibrium constants. In practice, a high concentration simulation is more efficient in that we are able to capture the behavior relevant to all lower concentrations, so long as the high concentration is not near the solubility limit.

To assess if there are significant differences in clustering as anion/cation size increases, we analyzed the results from simulations of 1 *m* KBr, NaBr, RbBr, RbCl, CsBr, and CsCl. Each electrolyte has its own intrinsic set of equilibrium constants presented in Tables 4 and 5. The cluster populations, measured directly from simulation at 1 *m* and estimated on the basis of equilibrium constants for lower concentrations, are graphed in Figure 5 for the nonrubidium electrolytes studied in this work. The equilibrium constants shown in Tables 4 and 5 lead to a prediction of statistically insignificant pairing and cluster formation for concentrations below 0.1 *m* and complete dissociation in the infinite dilution limit. However, as concentrations approach 1 *m*, there are significant differences in the clustering propensities between different salts. For example, for a concentration of 1 *m*, approximately 22% of ions in the Cl^- and Br^- salts of Na^+, K^+, and Cs^+ are involved in ion pairs. However, the degree of dissociation is different between these salts because of differences in populations for higher order clusters. This is illustrated through a direct comparison between 1 *m* NaCl to 1 *m* CsCl. For the former, 24% of the ions participate in triplets or higher order clusters, whereas this number is 11% for CsCl.

We analyzed the detailed inventory of microscopic equilibrium constants shown in Tables 4 and 5 to uncover a set of rules for unilateral (addition of a single anion or cation) and bilateral (addition of an ion pair) associations. This analysis revealed the following trends: 1. Unilateral associations are favorable if the process results in a cluster with a reduced net charge. To illustrate this point, we draw attention to magnitudes of equilibrium constants such as, $k_{2,3}^{(c)}$, $k_{3,2}^{(a)}$, and $k_{3,4}^{(c)}$. 2. Unilateral associations are unfavorable if the process results in a cluster of increased net charge. Examples of unfavorable unilateral associations are seen in values for $k_{1,2}^{(a)}$, $k_{1,3}^{(a)}$, and so forth, which also follow the trend that $k_{1,2}^{(a)} > k_{1,3}^{(a)} \gg \ldots$ and $k_{1,2}^{(a)} > k_{1,3}^{(a)} \gg \ldots$. 3. The dominant preference is for dissociated species, followed by pairs, and then the larger clusters. Equilibrium constants for bilateral associations are typically less than unity.

The equilibrium constants shown in Tables 4 and 5 also allow us to estimate the free energies of different cluster species with respect to each other and with respect to the fully dissociated species. The calculated values were used to construct a free energy landscape as shown in Figure 6. The reference state ($\Delta G = 0$) is that of the completely dissociated ion. Three distinct

TABLE 3: Ion Pair and Cluster Equilibrium Constants Computed from Molecular Dynamics Simulations of NaCl at Different Concentrations[a]

	Concentration				
	100 m*m*	250 m*m*	500 m*m*	750 m*m*	1 *m*
$k_{1,1}$ (m^{-1})	0.86 ± 0.10	0.77 ± 0.06	0.78 ± 0.05	0.77 ± 0.05	0.76 ± 0.05
$k_{1,2}^{(a)}$ (m^{-1})		0.20 ± 0.06	0.25 ± 0.03	0.25 ± 0.03	0.25 ± 0.03
$k_{1,2}^{(c)}$ (m^{-1})		0.19 ± 0.05	0.28 ± 0.04	0.28 ± 0.03	0.29 ± 0.03
$k_{2,2}^{(a)}$ (m^{-1})			1.39 ± 0.31	1.26 ± 0.31	1.32 ± 0.18
$k_{2,2}^{(c)}$ (m^{-1})			1.24 ± 0.25	1.15 ± 0.25	1.16 ± 0.16
$k_{2,2}^{(p)}$ (m^{-1})			0.45 ± 0.09	0.41 ± 0.09	0.44 ± 0.06
$k_{1,3}^{(a)}$ (m^{-1})				0.14 ± 0.06	0.13 ± 0.04
$k_{3,1}^{(c)}$ (m^{-1})				0.10 ± 0.05	0.11 ± 0.03
$k_{2,3}^{(a)}$ (m^{-1})				0.45 ± 0.13	0.48 ± 0.10
$k_{2,3}^{(c)}$ (m^{-1})				3.94 ± 1.87	4.91 ± 1.70
$k_{2,3}^{(p)}$ (m^{-1})				0.73 ± 0.21	0.83 ± 0.18
$k_{3,2}^{(a)}$ (m^{-1})				5.24 ± 2.68	5.20 ± 1.64
$k_{3,2}^{(c)}$ (m^{-1})				0.44 ± 0.12	0.50 ± 0.10
$k_{3,2}^{(p)}$ (m^{-1})				0.66 ± 0.18	0.77 ± 0.16
$k_{3,3}^{(a)}$ (m^{-1})				1.38 ± 0.51	1.23 ± 0.34
$k_{3,3}^{(c)}$ (m^{-1})				1.36 ± 0.53	1.30 ± 0.37
$k_{3,3}^{(p)}$ (m^{-1})				0.80 ± 0.25	0.81 ± 0.20

[a] Blank entries indicate that no statistically significant information could be extracted regarding the cluster in question. Error bars were extracted from bootstrap analysis as described in Methods. Data in the table show that equilibrium constants are invariant to changes in concentration. Similar results regarding the invariance of equilibrium constants were obtained for KCl as well (data not shown).

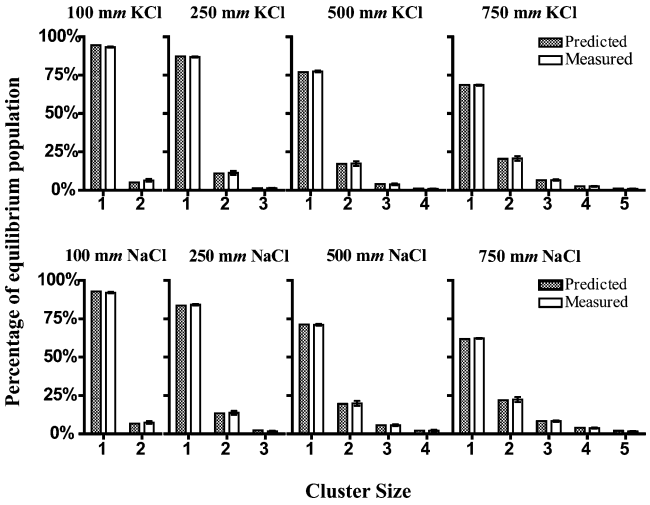

Figure 4. Comparison of average cluster populations measured from simulation data (white bars) to those predicted using equilibrium constants (textured bars) extracted from 1 *m* simulations of NaCl and KCl. The predictions were made using the average equilibrium constants derived from Table 4, and it is seen that the standard error in the measured populations are small and the predicted populations are in very good agreement with the measured populations.

observations emerge from inspection of the free energy landscapes shown in Figure 6: First, clusters with a net neutral charge, namely, pairs, quadruplets which are pairs of pairs, and so forth, are thermodynamically favored over clusters with a net charge. Second, ion pairing makes significant contributions to electrolyte free energy landscapes for all of the salts shown in Figure 6. This quantitative characterization of ion pairing may help resolve some of the continued speculation about the importance of ion pairing in strong 1:1 electrolytes. Third, while pairing is of equivalent importance for all of the salts shown in Figure 6, the degree to which larger clusters are favored depends markedly on the type of cation. Specifically, the likelihood of forming large clusters decreases with increasing cation size. A comparison with the simulation data of Koneshan et al.[55] shows that the calculated propensities of a Group I cation for pairing and clustering correlate with the affinity of the ion for its primary hydration shell; that is, the greater the affinity of a cation is for its primary hydration shell, the higher the propensity is to form pairs and clusters. This suggests that ion pairing and clustering results from a balance between two favorable enthalpic processes.

Comparison to Estimates from Conductometric Experiments. Although there is no direct experimental verification for the higher order association constants, we were able to compare the pair association constants ($k_{1,1}$) computed using our simulation data to those obtained by Fuoss et al.[9] These comparisons are shown in Table 6. The agreement between numbers estimated from simulation and those arrived at using conductometry is very good for NaCl, NaBr, KCl, and CsBr. The agreement is satisfactory for KBr and CsCl and poor for the two rubidium salts we have studied.

Favorable comparison between estimates for ion pairing from simulation versus conductometric data for strong 1:1 electrolytes suggests that there is a direct connection between the types of data used in the parametrization and the physical basis for ion pairing. Aqvist modeled anions and cations as soft spheres with surface charge. The Lennard−Jones parameters were tuned to recapitulate free energies of hydration and the position of the first peak for water−cation RDFs.[42] Accuracy of the parameters was assessed by comparing calculated enthalpies for gas-phase monohydrates to estimates from experiment. Pairing is a balance between the favorable unshielded Coulomb interactions and the unfavorable partial desolvation of ion pairs; it logically follows that, for monovalent ions, the former is dictated by the ionic radius, that is, the surface charge density, while the latter is determined by the hydration free energy. In light of the preceding discussion, it seems less surprising that simulations based on Aqvist's parameters lead to quantitative agreement for estimates of ion pairing from conductometric measurements. The paradigm should be worse for processes that go beyond the balance of unshielded Coulomb interactions and dehydration. For example, Grossfield et al.[56] find that Aqvist's parameters are not adequate for describing the free energies for transfer of monovalent ions between different media. This inadequacy is attributed to the lack of polarizability in the Aqvist paradigm.

TABLE 4: Microscopic Equilibrium Constants Extracted from Simulations of 1 *m* Alkali-Chloride Salts[a]

equilibrium constant (m^{-1})	NaCl	KCl	RbCl	CsCl
$k_{1,1}$	0.76 ± 0.06	0.57 ± 0.04	0.52 ± 0.12	0.49 ± 0.07
$k_{1,2}^{(a)}$	0.26 ± 0.03	0.19 ± 0.02	0.17 ± 0.06	0.16 ± 0.03
$k_{1,3}^{(a)}$	0.13 ± 0.05	0.07 ± 0.02	0.07 ± 0.02	0.06 ± 0.01
$k_{2,1}^{(c)}$	0.29 ± 0.04	0.22 ± 0.02	0.18 ± 0.06	0.15 ± 0.03
$k_{3,1}^{(c)}$	0.11 ± 0.04	0.10 ± 0.02	0.07 ± 0.02	0.06 ± 0.02
$k_{2,2}^{(a)}$	1.16 ± 0.20	0.94 ± 0.11	0.81 ± 0.27	0.73 ± 0.15
$k_{2,2}^{(c)}$	1.28 ± 0.23	1.05 ± 0.12	0.85 ± 0.28	0.70 ± 0.15
$k_{2,2}^{(p)}$	0.44 ± 0.08	0.35 ± 0.05	0.29 ± 0.11	0.23 ± 0.06
$k_{2,3}^{(a)}$	0.44 ± 0.14	0.32 ± 0.05	0.31 ± 0.11	0.26 ± 0.06
$k_{2,3}^{(c)}$	4.48 ± 1.98	4.68 ± 1.31	3.88 ± 1.37	2.99 ± 0.74
$k_{2,3}^{(p)}$	0.75 ± 0.22	0.58 ± 0.10	0.51 ± 0.21	0.37 ± 0.10
$k_{2,4}^{(a)}$	0.24 ± 0.18	0.12 ± 0.06	0.12 ± 0.05	0.12 ± 0.04
$k_{2,4}^{(c)}$	1.43 ± 1.13	0.94 ± 0.51	0.89 ± 0.42	0.73 ± 0.28
$k_{3,2}^{(a)}$	5.16 ± 2.29	3.78 ± 0.78	3.91 ± 1.47	3.08 ± 0.83
$k_{3,2}^{(c)}$	0.48 ± 0.14	0.39 ± 0.06	0.32 ± 0.11	0.25 ± 0.06
$k_{3,2}^{(p)}$	0.74 ± 0.20	0.64 ± 0.11	0.50 ± 0.21	0.38 ± 0.10
$k_{3,3}^{(a)}$	1.25 ± 0.49	0.92 ± 0.18	0.86 ± 0.30	0.70 ± 0.19
$k_{3,3}^{(c)}$	1.37 ± 0.56	1.13 ± 0.23	0.89 ± 0.31	0.68 ± 0.18
$k_{3,3}^{(p)}$	0.80 ± 0.28	0.63 ± 0.12	0.53 ± 0.22	0.36 ± 0.10
$k_{3,4}^{(a)}$	0.62 ± 0.32	0.36 ± 0.15	0.36 ± 0.14	0.34 ± 0.13
$k_{3,4}^{(c)}$	3.47 ± 2.85	3.52 ± 2.14	2.64 ± 1.15	1.94 ± 0.84
$k_{3,4}^{(p)}$	1.11 ± 0.57	0.71 ± 0.29	0.61 ± 0.27	0.48 ± 0.18
$k_{3,5}^{(a)}$			0.20 ± 0.12	0.18 ± 0.12
$k_{3,5}^{(p)}$			1.01 ± 0.67	0.70 ± 0.49
$k_{4,2}^{(c)}$	0.24 ± 0.15	0.16 ± 0.06	0.16 ± 0.07	0.11 ± 0.04
$k_{4,2}^{(p)}$	1.61 ± 1.11	1.07 ± 0.43	1.18 ± 0.64	0.69 ± 0.30
$k_{4,3}^{(a)}$	3.29 ± 2.37	2.52 ± 1.13	1.93 ± 1.11	2.04 ± 0.96
$k_{4,3}^{(c)}$	0.62 ± 0.33	0.45 ± 0.14	0.36 ± 0.17	0.32 ± 0.12
$k_{4,3}^{(p)}$	1.03 ± 0.51	0.72 ± 0.22	0.58 ± 0.31	0.46 ± 0.17
$k_{4,4}^{(a)}$	1.30 ± 0.86	0.87 ± 0.40	0.80 ± 0.44	0.76 ± 0.37
$k_{4,4}^{(c)}$	1.31 ± 0.87	1.08 ± 0.57	0.80 ± 0.37	0.70 ± 0.35
$k_{4,4}^{(p)}$	1.07 ± 0.63	0.68 ± 0.28	0.55 ± 0.27	0.49 ± 0.23
$k_{4,5}^{(a)}$		0.42 ± 0.35	0.46 ± 0.41	0.38 ± 0.23
$k_{4,5}^{(p)}$		0.80 ± 0.65	0.70 ± 0.63	0.55 ± 0.32
$k_{5,3}^{(c)}$				0.12 ± 0.08
$k_{5,3}^{(p)}$				0.48 ± 0.37
$k_{5,4}^{(a)}$				1.82 ± 1.59
$k_{5,4}^{(c)}$		0.51 ± 0.37	0.50 ± 0.31	0.28 ± 0.19
$k_{5,4}^{(p)}$		0.77 ± 0.53	0.77 ± 0.53	0.43 ± 0.29

[a] The notations for equilibrium constants are shown in Figure 3. Statistically insignificant measurements are left blank.

TABLE 5: Microscopic Equilibrium Constants Extracted from Simulations of 1 *m* Alkali-Bromide Salts[a]

equilibrium constant (m^{-1})	NaBr	KBr	RbBr	CsBr
$k_{1,1}$	0.72 ± 0.17	0.65 ± 0.10	0.60 ± 0.14	0.55 ± 0.14
$k_{1,2}^{(a)}$	0.22 ± 0.07	0.21 ± 0.05	0.19 ± 0.06	0.17 ± 0.06
$k_{1,3}^{(a)}$	0.12 ± 0.04	0.07 ± 0.02	0.08 ± 0.03	0.06 ± 0.02
$k_{2,1}^{(c)}$	0.27 ± 0.09	0.25 ± 0.06	0.21 ± 0.07	0.17 ± 0.06
$k_{3,1}^{(c)}$	0.10 ± 0.03	0.11 ± 0.03	0.08 ± 0.03	0.06 ± 0.02
$k_{2,2}^{(a)}$	1.03 ± 0.35	1.02 ± 0.23	0.93 ± 0.30	0.82 ± 0.29
$k_{2,2}^{(c)}$	1.23 ± 0.41	1.19 ± 0.27	1.00 ± 0.33	0.80 ± 0.29
$k_{2,2}^{(p)}$	0.38 ± 0.16	0.39 ± 0.11	0.32 ± 0.13	0.25 ± 0.11
$k_{2,3}^{(a)}$	0.48 ± 0.17	0.36 ± 0.09	0.33 ± 0.11	0.28 ± 0.10
$k_{2,3}^{(c)}$	4.85 ± 1.80	6.06 ± 1.68	4.25 ± 1.53	3.58 ± 1.43
$k_{2,3}^{(p)}$	0.83 ± 0.34	0.65 ± 0.19	0.55 ± 0.22	0.40 ± 0.18
$k_{2,4}^{(a)}$	0.14 ± 0.08	0.13 ± 0.04	0.12 ± 0.06	0.11 ± 0.06
$k_{2,4}^{(c)}$	0.96 ± 0.60	1.20 ± 0.47	0.86 ± 0.45	0.73 ± 0.41
$k_{3,2}^{(a)}$	4.04 ± 1.50	3.87 ± 0.96	3.86 ± 0.37	3.78 ± 0.48
$k_{3,2}^{(c)}$	0.37 ± 0.13	0.42 ± 0.10	0.35 ± 0.12	0.27 ± 0.10
$k_{3,2}^{(p)}$	0.54 ± 0.22	0.66 ± 0.19	0.55 ± 0.22	0.40 ± 0.18
$k_{3,3}^{(a)}$	1.53 ± 0.67	1.01 ± 0.25	0.93 ± 0.34	0.80 ± 0.32
$k_{3,3}^{(c)}$	1.19 ± 0.52	1.20 ± 0.30	1.00 ± 0.37	0.78 ± 0.32
$k_{3,3}^{(p)}$	0.80 ± 0.39	0.66 ± 0.19	0.55 ± 0.23	0.39 ± 0.18
$k_{3,4}^{(a)}$	0.28 ± 0.15	0.43 ± 0.13	0.34 ± 0.15	0.37 ± 0.20
$k_{3,4}^{(c)}$	2.32 ± 1.50	4.05 ± 1.53	2.83 ± 1.47	2.57 ± 1.56
$k_{3,4}^{(p)}$	0.46 ± 0.24	0.80 ± 0.27	0.57 ± 0.27	0.53 ± 0.30
$k_{3,5}^{(a)}$	0.54 ± 0.49	0.21 ± 0.14	0.16 ± 0.13	0.22 ± 0.20
$k_{3,5}^{(p)}$	1.75 ± 1.71	1.32 ± 0.91	0.77 ± 0.66	1.00 ± 0.94
$k_{4,2}^{(c)}$	0.12 ± 0.09	0.20 ± 0.06	0.17 ± 0.06	0.11 ± 0.05
$k_{4,2}^{(p)}$	0.66 ± 0.53	1.20 ± 0.39	1.07 ± 0.50	0.73 ± 0.41
$k_{4,3}^{(a)}$	7.13 ± 5.65	2.85 ± 0.92	2.61 ± 1.06	2.51 ± 1.28
$k_{4,3}^{(c)}$	0.55 ± 0.26	0.57 ± 0.17	0.46 ± 0.18	0.33 ± 0.14
$k_{4,3}^{(p)}$	1.17 ± 0.55	0.88 ± 0.29	0.72 ± 0.31	0.49 ± 0.23
$k_{4,4}^{(a)}$	0.83 ± 0.59	0.97 ± 0.35	0.94 ± 0.47	0.75 ± 0.38
$k_{4,4}^{(c)}$	1.64 ± 1.23	1.27 ± 0.47	1.28 ± 0.70	0.67 ± 0.40
$k_{4,4}^{(p)}$	0.63 ± 0.48	0.84 ± 0.31	0.73 ± 0.41	0.45 ± 0.25
$k_{4,5}^{(a)}$	1.51 ± 1.26	0.44 ± 0.20	0.46 ± 0.33	0.32 ± 0.25
$k_{4,5}^{(p)}$	3.45 ± 2.44	0.86 ± 0.39	0.99 ± 0.70	0.40 ± 0.33
$k_{5,3}^{(c)}$		0.28 ± 0.14	0.18 ± 0.13	
$k_{5,3}^{(p)}$		1.22 ± 0.64	0.77 ± 0.60	
$k_{5,4}^{(a)}$		2.59 ± 1.39	3.37 ± 2.66	
$k_{5,4}^{(c)}$		0.75 ± 0.30	0.63 ± 0.38	
$k_{5,4}^{(p)}$		1.11 ± 0.46	1.00 ± 0.55	
$k_{5,5}^{(a)}$		0.76 ± 0.41	0.86 ± 0.67	
$k_{5,5}^{(c)}$		1.29 ± 0.73	1.18 ± 1.04	
$k_{5,5}^{(p)}$		0.87 ± 0.49	0.91 ± 0.74	

[a] The notations for equilibrium constants are as shown in Figure 3.

The discrepancy between simulation and experimental data for rubidium merits further discussion. Specifically, we predict greater ion pairing and clustering vis-à-vis experiments. We attribute this inaccuracy to inadequacies in the forcefield parameters for rubidium. This proposal is reasonable in light of the fact that neither X-ray nor neutron scattering data were available for rubidium salts at the time of parametrization.[42] In the Aqvist paradigm, this information provides a second constraint for tuning the Lennard−Jones parameters.

The ability to explain experimental observations of nonidealities in electrolytes bodes well for their use in simulations of ion and co-ion effects around macromolecules such as RNA and DNA. On the basis of quantitative comparisons to conductometric data, we conclude that the parameters for Na^+, K^+, Cs^+, Cl^-, and Br^- ions are reasonably robust for simulations of NaCl, KCl, NaBr, and CsBr, while other combinations should be used with some caution. We propose that a systematic sensitivity analysis combined with the Aqvist paradigm, whereby the Lennard−Jones parameters are tuned to achieve agreement with conductometric data, should lead to more reliable parameters for all Group I cations.

Kinetic Analysis of Desolvation Processes Associated with the Formation of Ion Pairs. The ion pair decorrelation function, $G_m(r, t)$, which was computed as described in Methods, can be well-fit to a biexponential decay process as shown in Figure 7a. Values for the two distinct time scales τ_1 and τ_2, which result from the fitting process, are shown in Table 7. These values were obtained from fits to data from simulations of 1 *m* solutions of all eight 1:1 electrolytes that we studied. We have found that the calculated time scales show very weak dependence on electrolyte concentration (data not shown). For the purposes of bootstrap analysis, the slowest process in our system corresponds to the time scale τ_2. This in turn dictates the number of truly independent snapshots one can obtain using a single trajectory. If a simulation is run for 10 ns, then there are approximately 10 ns/$2\tau_2$ independent snapshots within the trajectory.

From a fitting standpoint, the use of a biexponential is motivated by the large, nonrandom residuals resulting from a monoexponential fit. The residuals are shown as an inset in Figure 7a. However, goodness of fit alone cannot justify the use of a model that purports the existence of two distinct physical processes for ion pair formation/dissociation. Closer scrutiny reveals a simple physical explanation: The equilibrium cation−anion RDF (Figure 2a) contains a small secondary peak corresponding to the solvent-separated ion pair (SSIP). Analysis

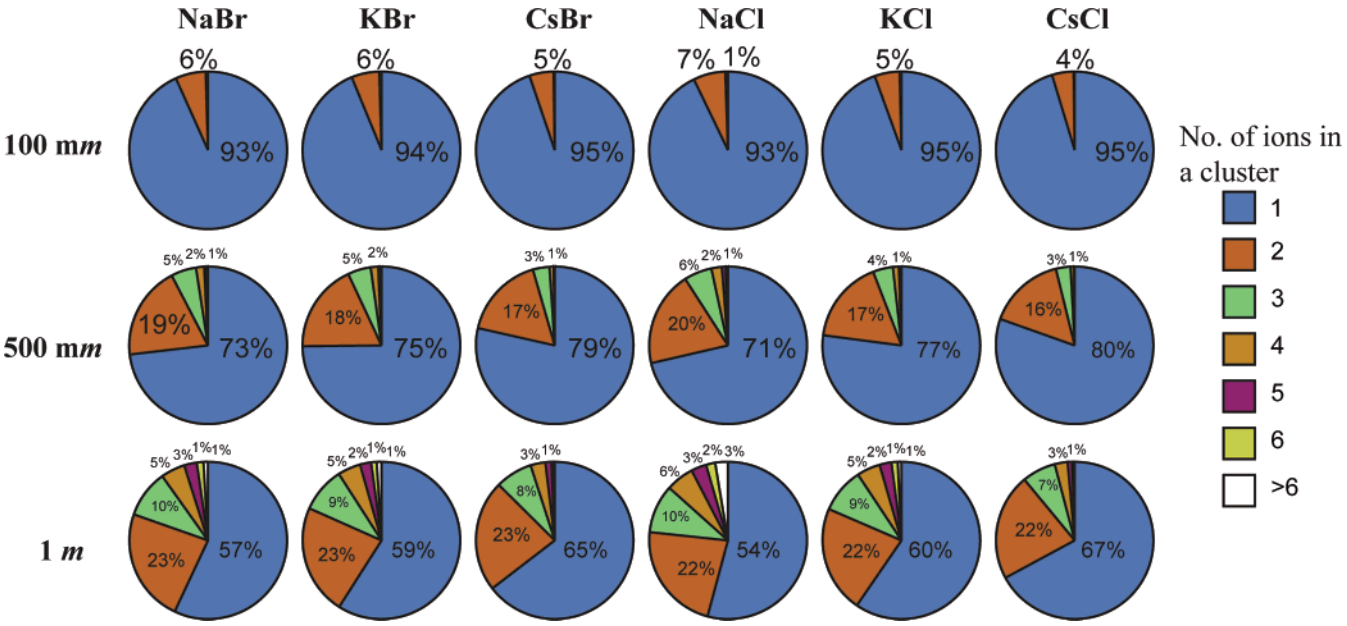

Figure 5. Distribution of cluster populations for Cl and Br salts of Na, K, and Cs. The 1 *m* populations are directly measured from simulation, while the lower concentration populations are predicted using the equilibrium constants extracted from the 1 *m* simulations. For the latter, we used the average values of equilibrium constants obtained from Tables 4 and 5; that is, the standard errors in these values were ignored in our estimation of cluster populations. This was done in the interest of clarity, and therefore, the pie charts serve only as devices for visualizing the extent of pairing and clustering expected in strong 1:1 electrolytes at different concentrations.

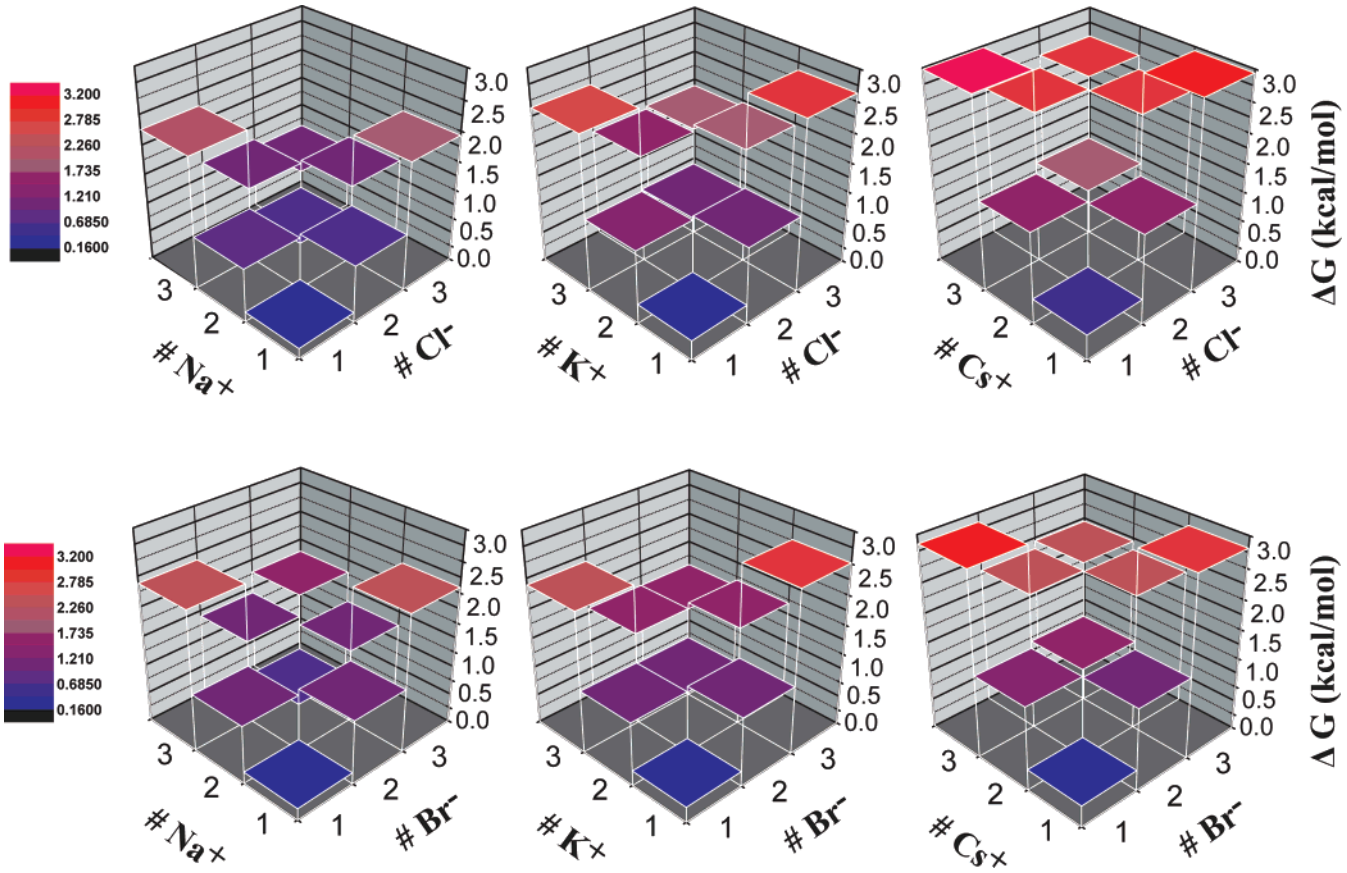

Figure 6. Free energy landscapes for 1 *m* NaCl, KCl, CsCl, NaBr, KBr, and CsBr. The reference state is the fully dissociated species. The landscape was constructed using the equilibrium constants shown in Tables 4 and 5 and shows relative free energies for all species up to sextuplets. The axes are the number of anions, number of cations, and the free energy of a particular species with respect to the dissociated species. A color bar each is used for the Cl^- and Br^- salts.

of the decay of the second peak of $G_m(r, t)$, shown in Figure 7b, reveals a buildup from zero population corresponding to the short decay time τ_1 followed by a uniform, monoexponential decay corresponding to τ_2. Therefore, the short lifetime τ_1 corresponds to a transition between the contact ion pair (CIP) and the SSIP. Conversely, the longer time scale τ_2 describes the relaxation of SSIPs to bulk ions and the concomitant loss of pair correlation.

TABLE 6: Comparison of Equilibrium Constants for Ion Pairing[a]

salt	$k_{1,1}$ from simulations (m^{-1})	$k_{1,1}$ from conductometry (m^{-1})
NaCl	0.76 ± 0.05	0.82
NaBr	0.72 ± 0.07	0.73
KCl	0.57 ± 0.04	0.53
KBr	0.65 ± 0.07	0.44
RbCl	0.52 ± 0.05	0.24
RbBr	0.60 ± 0.06	0.23
CsCl	0.48 ± 0.05	0.62
CsBr	0.55 ± 0.06	0.54

[a] Column two shows values obtained from simulations and these are compared to estimates from conductometric measurements

TABLE 7: Tabulation of Decorrelation Times for CIP (τ_1) and SSIP (τ_2) for Different 1:1 Electrolytes

salt	τ_1 (ps)	τ_2 (ps)
NaCl	96 ± 4	251 ± 8
NaBr	97 ± 5	239 ± 9
KCl	24 ± 1	93 ± 7
KBr	31 ± 1	113 ± 5
RbCl	21 ± 1	97 ± 5
RbBr	23 ± 1	97 ± 5
CsCl	15 ± 1	82 ± 5
CsBr	17 ± 1	88 ± 5

The stepwise dissociation mechanism discussed above is congruent with the mechanism proposed by Eigen and Tamm.[21] On the basis of ultrasonic absorption data for ionic solutions, they proposed a sequential multistage mechanism for the formation and breakdown of ion pairs. Their scheme is summarized using the convention proposed by Marcus and Efter.[1]

$$C^+S_m + A^-S_n \overset{k_1}{\rightleftharpoons} S_pC^+S_2A^-S_q \overset{k_2}{\rightleftharpoons} S_rC^+SA^-S_s \overset{k_3}{\rightleftharpoons} S_xC^+A^-S_y$$

$$m > p > r > x$$

$$n > q > s > y$$

$$m + n = p + q + 2 \qquad (4)$$

or

$$\text{solvated cation} + \text{solvated anion} \overset{k_1}{\rightleftharpoons} \text{2SIP} \overset{k_2}{\rightleftharpoons} \text{SSIP} \overset{k_3}{\rightleftharpoons} \text{CIP}$$

Here, C^+ denotes a monovalent cation, A^- denotes a monovalent anion, and S_i (where i is one of m, n, p, q, r, s, x, or y) refers to i solvent molecules. In the Eigen−Tamm mechanism, fully solvated, dissociated ions come together to form a diffusion-limited complex ($S_pC^+S_2A^-S_q$ or 2SIP) whereby two ions, with their solvation shells still intact, come into contact. The second step pertains to the release of one or more water molecules leading to the formation of a complex characterized by the sharing of a water molecule between the two ions. This is denoted as the SIP. The final step corresponds to the formation of a CIP.

It is encouraging that our kinetic analysis of simulation data clearly identifies the existence of two of the three species proposed by Eigen and Tamm,[21] namely, CIPs and SSIPs. There is no gain in accuracy if we use a triexponential to fit data for the decay of $G_m(r, t)$ and this suggests that, at least for our simulation data, the proposed 2SIP species is statistically indistinguishable from fully solvated ions in the bulk. Eigen and Tamm proposed that the formation and dissociation of this species is likely to be very rapid, approximately 2 ps. This time scale is similar in magnitude to the time constant used for coupling to the Berendsen thermostat and manostat.[45] Therefore, it is not unreasonable to find that in our simulations the 2SIP species is indistinguishable from bulk ions.

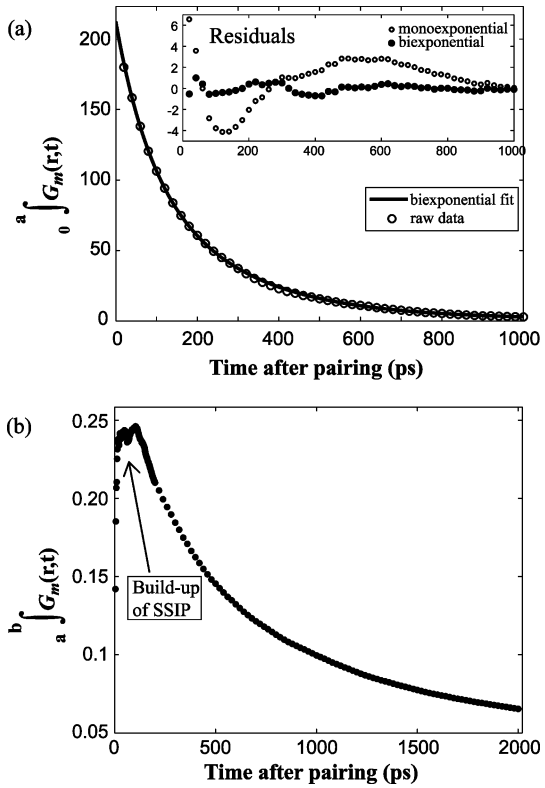

Figure 7. (a) Decay of the integral of $G_m(r, t)$ for NaCl (open circles); the upper limit for the integral, **a**, is the position of the first minimum of the pair correlation function shown in Table 2. The curve shows results of a biexponential fit to the data. Residuals for both mono and biexponential fits are shown as an inset. (b) Data showing the build-up and decay of the SSIP component of $G_m(r, t)$ (shown as solid circles). The upper limit for the integral, **b**, is set to be greater than $r_{\min}^{(2)}$ (see Table 2), which is the distance past which the equilibrium anion−cation RDF decays to unity.

Conclusions

We have shown that all-atom molecular dynamics simulations of aqueous strong 1:1 electrolytes reproducibly exhibit significant degrees of ion pairing and clustering. Pairing and clustering are a consequence of the balance between favorable electrostatic interactions and unfavorable partial desolvation of ions. Qualitatively, the observed mechanism for ion pairing is congruent with the multistep scheme of Eigen and Tamm.[21] For each 1:1 electrolyte, there exists a set of equilibrium constants to quantitatively describe the variation of cluster populations with electrolyte concentration. With the exception of rubidium salts, the values for pairing propensities agree with estimates from conductometric data. The degree of pairing is sufficiently small ($k_a < 1$) for all alkali−halides such that dilute solutions (<100 m*m*) are essentially completely dissociated. However, at high concentrations (≥ 1 *m*), more than a third of the alkali−halide ions are found to participate in a pair or cluster, with the proportions being specific to the type of salt. This could potentially explain why nonidealities of aqueous, 1:1 strong electrolytes are highly salt-specific despite convergence to the same limiting laws at infinite dilution. Finally, the tabulated equilibrium constants provide a quantitative thermodynamic framework for explaining differences in specific and nonspecific

ion binding to polyelectrolytes in monovalent salts. In recent work, Rösgen et al.[57] have extended the semi-grand ensemble approach of Hill[58,59] for the calculation of activity coefficients of two-component solutions. Their approach formally allows for the inclusion of pairing and clustering in the calculation of activity coefficients. In ongoing work, we are pursuing a tractable method for the calculation of activity coefficients based on the combined use of our equilibrium constants and the formalism of Rösgen et al.

Acknowledgment. We are grateful to Nathan Baker, David Draper, Kathleen Hall, Timothy Lohman, and Andreas Vitalis for many helpful discussions. This work was supported by Grant MCB 0416766 from the National Science Foundation. A.A.C. acknowledges partial support from the NIH through an NRSA training grant.

References and Notes

(1) Marcus, Y.; Hefter, G. *Chem. Rev.* **2006**, *106*, 4585.
(2) Kraus, C. A. *J. Phys. Chem.* **1956**, *60*, 129.
(3) Prue, J. E. Ion Association and Solvation. In *Chemical Physics of Ionic Solutions*; Conway, B. E., Barradas, R. G., Eds.; John Wiley: New York, 1966; p 163.
(4) Robinson, R. A.; Stokes, R. H. *Electrolyte Solutions*, 2nd revised ed.; Dover: Mineola, NY, 2002.
(5) Kraus, C. A. *J. Phys. Chem.* **1954**, *58*, 673.
(6) Scatchard, G. *Chem. Rev.* **1933**, *13*, 7.
(7) Szwarc, M. *Acc. Chem. Res.* **1969**, *2*, 87.
(8) Barthel, J. M. G.; Krienke, H.; Kunz, W. *Physical Chemistry of Electrolyte Solutions: Modern Aspects*; Springer: New York, 1998; Vol. 5.
(9) Fuoss, R. M. *Proc. Natl. Acad. Sci. U.S.A.* **1980**, *77*, 34.
(10) Oelkers, E. H.; Helgeson, H. C. *Science* **1993**, *261*, 888.
(11) Johnson, K. S.; Pytkowicz, R. M. Ion Association and Activity Coefficients in Multicomponent Solutions. In *Activity Coefficients on Electrolyte Solutions*; Pytkowicz, R. M., Ed.; CRC Press, Inc.: Boca Raton, FL, 1979; Vol. 2; p 36.
(12) Dillon, S. R.; Dougherty, R. C. *J. Phys. Chem. A* **2003**, *107*, 10217.
(13) Georgalis, Y.; Kierzek, A. M.; Saenger, W. *J. Phys. Chem. B* **2000**, *104*, 3405.
(14) Patra, M.; Karttunen, M. *J. Comput. Chem.* **2004**, *25*, 678.
(15) Koneshan, S.; Rasaiah, J. C. *J. Chem. Phys.* **2000**, *113*, 8125.
(16) Chowdhuri, S.; Chandra, A. *J. Chem. Phys.* **2001**, *115*, 3732.
(17) Sherman, D. M.; Collings, M. D. *Geochem. Trans.* **2002**, *3*, 102.
(18) Degrève, L.; da Silva, F. L. B. *J. Chem. Phys.* **1999**, *110*, 3070.
(19) Degrève, L.; da Silva, F. L. B. *J. Chem. Phys.* **1999**, *111*, 5150.
(20) Vieira, D. S.; Degrève, L. *J. Mol. Struct. Theochem* **2002**, *580*, 127.
(21) Eigen, M.; Tamm, K. *Z. Elektrochem.* **1962**, *66*, 93.
(22) Record, M. T., Jr.; Anderson, C. F.; Lohman, T. M. *Q. Rev. Biophys.* **1978**, *11*, 103.
(23) Tan, Z.-J.; Chen, S.-J. *J. Chem. Phys.* **2005**, *122*, 044903.
(24) Savelyev, A.; Papoian, G. A. *J. Am. Chem. Soc.* **2006**, *128*, 14506.
(25) Anderson, C. F.; Record, M. T., Jr. *Annu. Rev. Phys. Chem.* **1995**, *46*, 657.
(26) Debye, P.; Hückel, E. *Phys. Z.* **1923**, *24*, 185.
(27) Bjerrum, N. *K. Dan. Vidensk. Selsk.* **1926**, *7*, 1.
(28) Bockris, J. O. M.; Reddy, A. K. N. *Modern Electrochemistry*; Plenum: New York, 1973; Vol. 1.
(29) Kovalenko, A.; Hirata, F. *J. Chem. Phys.* **2000**, *112*, 10391.
(30) Perkyns, J. S.; Pettitt, B. M. *Chem. Phys. Lett.* **1992**, *190*, 626.
(31) Pettitt, B. M.; Rossky, P. J. *J. Chem. Phys.* **1982**, *77*, 1451.
(32) Onsager, L. *Phys. Z.* **1927**, *28*, 277.
(33) Fuoss, R. M.; Onsager, L. *Proc. Natl. Acad. Sci. U.S.A.* **1955**, *41*, 274.
(34) Fuoss, R. M.; Hsia, K.-L. *Proc. Natl. Acad. Sci. U.S.A.* **1967**, *57*, 1550.
(35) Fuoss, R. M. *J. Phys. Chem.* **1975**, *79*, 525.
(36) Fuoss, R. M. *J. Phys. Chem.* **1975**, *79*, 1983.
(37) Fuoss, R. M. *J. Am. Chem. Soc.* **1978**, *100*, 5576.
(38) Fuoss, R. M. *J. Phys. Chem.* **1978**, *82*, 2427.
(39) Fuoss, R. M. *J. Am. Chem. Soc.* **1935**, *57*, 2604.
(40) Fuoss, R. M.; Kraus, C. A. *J. Am. Chem. Soc.* **1933**, *55*, 2387.
(41) Jorgensen, W. L.; Maxwell, D. S.; Tirado-Rives, J. *J. Am. Chem. Soc.* **1996**, *118*, 11225.
(42) Aqvist, J. *J. Phys. Chem.* **1990**, *94*, 8021.
(43) Jorgensen, W. L.; Chandrasekhar, J.; Madura, J. D.; Impey, R. W.; Klein, M. L. *J. Phys. Chem.* **1983**, *79*, 926.
(44) van der Spoel, D.; Lindahl, E.; Hess, B.; Groenhof, G.; Mark, A. E.; Berendsen, H. J. C. *J. Comput. Chem.* **2005**, *26*, 1701.
(45) Berendsen, H. J. C.; Postma, J. P. M.; van Gunsteren, W. F.; DiNola, A.; Haak, J. R. *J. Chem. Phys.* **1984**, *81*, 3684.
(46) Hockney, R. W.; Eastwood, J. W. *Computer Simulations Using Particles*; McGraw-Hill: New York, 1981.
(47) Miyamoto, S.; Kollman, P. A. *J. Comput. Chem.* **1992**, *13*, 952.
(48) Ponomarev, S. Y.; Thayer, K. M.; Beveridge, D. L. *Proc. Natl. Acad. Sci. U.S.A.* **2004**, *101*, 14771.
(49) King, G.; Warshel, A. *J. Chem. Phys.* **1989**, *91*, 3647.
(50) Kastenholz, M. A.; Hünenberger, P. H. *J. Phys. Chem. B* **2004**, *108*, 774.
(51) Darden, T.; York, D.; Pedersen, L. *J. Chem. Phys.* **1993**, *98*, 10089.
(52) van Hove, L. *Phys. Rev.* **1954**, *95*, 249.
(53) Arrhenius, S. *Z. Phys. Chem.* **1887**, *1*, 631.
(54) Degrève, L. *J. Chem. Soc., Faraday Trans. 2* **1988**, *84*, 1645.
(55) Koneshan, S.; Rasaiah, J. C.; Lynden-Bell, R. M.; Lee, S. H. *J. Phys. Chem. B* **1998**, *102*, 4193.
(56) Grossfield, A.; Ren, P.; Ponder, J. W. *J. Am. Chem. Soc.* **2003**, *125*, 15671.
(57) Rösgen, J.; Pettitt, B. M.; Perkyns, J. S.; Bolen, D. W. *J. Phys. Chem. B* **2004**, *108*, 2048.
(58) Hill, T. L. *J. Am. Chem. Soc.* **1957**, *79*, 4885.
(59) Hill, T. L. *J. Chem. Phys.* **1959**, *30*, 93.
(60) Chandrasekhar, J.; Spellmeyer, D. C.; Jorgensen, W. L. *J. Am. Chem. Soc.* **1984**, *106*, 903.
(61) Lybrand, T. P.; Ghosh, I.; McCammon, J. A. *J. Am. Chem. Soc.* **1985**, *107*, 7793.